Symbiotic Ambient Backscatter IoT Transmission over NOMA-Enabled Network

Mohamed Elsayed[1], Ahmed Samir[1], Ahmad A.Aziz El-Banna[1], Khaled Rabie[2],
Xingwang Li[3], Basem M. ElHalawany [1,4]
[1]Faculty of Engineering at Shoubra, Benha University, Egypt
[2] Department of Engineering, Manchester Metropolitan University, Manchester, UK
[3]School of Physics and Electronic Information Engineering, Henan Polytechnic University, China
[4]Corresponding Author
Emails: {mohamed.elsayed, ahmed.saied, ahmad.elbanna, basem.mamdoh}@feng.bu.edu.eg,
k.rabie@mmu.ac.uk, lixingwangbupt@gmail.com.

***Abstract*—Non-orthogonal multiple access (NOMA) and ambient backscatter communication (AmBC) play major roles to enhance spectrum efficiency in wireless communication systems. Besides, the AmBC provides good reinforcement for the current trend towards dispensing batteries for battery-free Internet-of-Things (IoT) devices. In this paper, we propose a symbiotic battery-free IoT system, that exploits the downlink transmission of a NOMA multiplexing enabled cellular network, to permit an IoT spectrum-efficient uplink communication. The IoT backscatter device (BD) performs a symbiotic radio (SR) relation with the cellular source to power its communication by intelligently reflecting the received power. We derive a closed-form expression of the ergodic capacity (EC) of the BD transmission and tight approximations of the ECs of the cellular source transmission, where all channels undergo Nakagami-*m* fading. Additionally, we validate the analytical results obtained using Monte-Carlo simulations. The influences of several system parameters such as power allocation factor, reflection coefficient, and channels' severity factors have been investigated. Finally, the performance of the proposed system is compared with a benchmark OMA-based system to highlight the achievable performance improvement.**

***Index Terms*—Internet-of-Things, non-orthogonal multiple access, ambient backscatter communication, symbiotic radio, ergodic capacity, Nakagami-*m* fading.**

I. Introduction

Signals multiplexing plays an essential role in developing spectrum utilization efficiency and raising the total system data rate. Unlike traditional orthogonal multiple access (OMA) techniques, Non-orthogonal multiple access (NOMA) enables the system to multiplex different data symbols, intended for single or multi-users, on the same time slot, frequency band, and spreading code [1], [2]. Although, researchers have proposed many types of NOMA, the power-domain NOMA (PD-NOMA) is the most widely used type. This technology relies on the idea of multiplexing data at different power levels at the transmitter while implementing a successive interference cancellation (SIC) to separate them at the receiver.

Ambient backscatter communication (AmBC) is another key technology that enables battery-free backscattering devices (BD) to use the ambient signals, which are abundantly available in the surrounding environment, as a carrier for its transmission process [3]–[6]. The ambient signal source, backscatter device (BD), and reader are the basic components of the AmBC system. The BD reflects the ambient signal after modulating it, by varying its antenna reflection coefficient [3]. As the AmBC requires neither dedicated battery nor radio resources, researchers consider it to be a promising technology to support low-cost and sustainable IoT devices. The authors in [7] proposed another type of AmBC systems, namely the symbiotic radio (SR). In SR, the ambient source performs a symbiotic relation with BD by powering the BD transmission, and the receiver decodes the information from the source as well as the BD. Different from AmBC, SR not only shares the source power and the spectrum of the main transmission but also shares the receiver. Thus, the SR system can enhance the performance by simultaneously supporting both transmissions.

To reap off advantage of the above-mentioned benefits, the combination of AmBC/SR and NOMA is a promising direction to enhance the performance of data transmission for massive IoT networks [8]. An example of such system was presented in [9], [10]. In [9], the authors proposed an optimization problem to get optimal values of reflection coefficient at BD, the transmitted power and the power allocation factors at source for enhancing the system ergodic capacity, while in [10], they evaluated the system performance in terms of the outage probabilities and the ergodic capacities for a NOMA-based SR network under Rayleigh fading channels. The authors in [11]–[13] analyzed the performance of NOMA based AmBC systems showing the trade-off between reliability and security. In [11], the physical layer security (PLS) of the AmBC-NOMA systems is investigated in the presence of a passive eavesdropper. The authors derived the outage probability and the intercept probability under the effect of hardware impairments and channel estimation uncertainty. Also in [12], authors illustrated the result of in-phase and quadrature-phase imbalance on the PLS of the same system. Finally, in [13], the reliability and security of a NOMA-based AmBC network were studied in the existence of a cognitive user. The secondary transmitter and BD aim to communicate with the legitimate user in the existence of an eavesdropper.

In this paper, we propose a downlink NOMA-based SR-AmBC system to improve the spectrum efficiency, where the cellular source adopts NOMA for multiplexing two messages intended for a single destination via a direct link while the BD exploits the cellular source signal as a carrier of its own information to send it towards the same destination. The main

differences between this work and [10], is that the former considers a NOMA multiplexing system, where the source multiplexes two symbols for the same destination, while the source in [10] exploits NOMA to deliver the information to two different destinations. Additionally, we consider a more generalized channel fading model namely, the Nakagami-*m*. Nakagami-*m* fading is very versatile as we can change its *m* for modeling different types of channel fading. To the best of our knowledge, no previous work implemented SR-AmBC based on NOMA as a multiplexing technique while the channels undergoes Nakagami-*m* fading.

The main contributions of this paper can be summarized as follows: (1) We derive closed-form expression of the EC of the BD transmission and tight approximations of the ECs of the cellular source transmission assuming that the wireless channels are characterized by Nakagami-*m* fading with an additive white Gaussian noise (AWGN). (2) Validate the analytical derivations through extensive Monte-Carlo simulations, and then we study the impact of system parameters on the system EC. (3) Finally, we carried out a comparison between the performance of the proposed system with a benchmark system.

The rest of this paper is organized as follows. The system model is introduced in Section II. The performance of considered system is evaluated in terms of the ergodic capacity are derived in Section III. Analytical and simulation results are discussed and compared with a bench mark system in Section IV and our conclusions are provided in Section V.

II. System Model

In this work, we consider the downlink NOMA-based SR-AmBC system shown in Fig.1. The system consists of a source node (S), backscatter device (BD), and a destination node (D). The transmitted power from S is used to convey its own multiplexed messages besides supporting the BD in transmitting its information simultaneously. For the sake of improving the spectrum efficiency, we assume that S adopts NOMA for multiplexing two messages, x_1 and x_2, intended for a single destination D directly [14], [15]. On the other hand, the BD exploits this ambient signal as a carrier of its own message x_3 by reflecting and modulating the received signal towards the same destination. The BD symbolizes a battery-free IoT device, which symbiotically coexists with the conventional transmitter S. In this Paper, we have assumed that the CSI is available at D. All channels are characterized by Nakagami-*m* fading under AWGN noise.

Following the NOMA principle, the transmitted message from S to D is expressed as $x_S = \sqrt{a_1 P}\ x_1 + \sqrt{a_2 P}\ x_2$, where P denotes the total transmitted power of the source S, and a_i denotes the power allocation factor for the messages x_i for $i \in \{1, 2\}$. Without loss of generality, it can be assumed that $a_1 > a_2$ and satisfy the condition $a_1 + a_2 = 1$. Then the received signal at D is given as $y = h_{SD}\ x_S + \sqrt{\beta}\ h_{BD}\ h_{SB}\ x_S\ x_3 + n$, where h_{SD}, h_{SB}, and h_{BD} denote the fading of the Nakagami-*m* wireless channels with severity factor m_j and $j \in \{SD, SB, BD\}$, respectively.

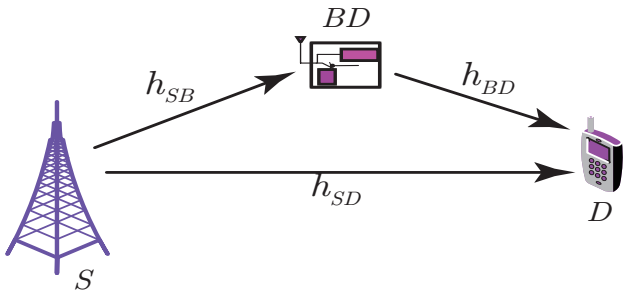

Figure 1. Downlink NOMA-based SR-AmBC system model

The expectations of the channels gains are $E\left[|h_j|^2\right] = \Omega_j$, n denotes AWGN with zero mean and σ^2 variance, and β is the BD reflection coefficient. Therefore, the received signal to interference plus noise ratio (SINR) at D to detect x_1 is

$$\gamma_1 = \frac{a_1 \rho |h_{SD}|^2}{a_2 \rho |h_{SD}|^2 + \beta \rho |h_{SB}|^2 |h_{BD}|^2 + 1}, \tag{1}$$

where $\rho = \frac{P}{\sigma^2}$ is the transmitted signal to noise ratio (SNR) at S. Under the assumption of perfect SIC, the SINR for detecting x_2 message is given as

$$\gamma_2 = \frac{a_2 \rho |h_{SD}|^2}{\beta\ \rho\ |h_{SB}|^2 |h_{BD}|^2 + 1}. \tag{2}$$

Again D can perform another SIC assuming that $\beta < a_i$ where the SINR for detecting x_3 message is given as

$$\gamma_3 = \beta\ \rho\ |h_{SB}|^2 |h_{BD}|^2 \tag{3}$$

Channels Distributions: Given a Nakagami-*m* distributed wireless channel h_j, the channel gain, $|h_j|^2$, undergoes a Gamma distribution with probability density function (PDF) and cumulative distribution function (CDF) given respectively as follows, assuming that the fading parameter m_j is an integer value greater than or equal to one [16], [17],

$$f_{|h_j|^2}(x) = \left(\frac{m_j}{\Omega_j}\right)^{m_j} \frac{x^{m_j - 1}}{\Gamma(m_j)} e^{\left(\frac{-m_j}{\Omega_j} x\right)}, \tag{4}$$

$$F_{|h_j|^2}(x) = 1 - e^{\left(\frac{-m_j}{\Omega_j} x\right)} \sum_{m=0}^{m_j - 1} \frac{((m_j/\Omega_j)x)^m}{m!}, \tag{5}$$

where $\Gamma(.)$ is the gamma function. On the other hand, the PDF and CDF of the product of two squared Nakagami-*m* random variables, $\nu = |h_{SB}|^2 |h_{BD}|^2$, is given as follows [18] [19],

$$f_{|v|^2}(v) = \frac{2\ v^{\frac{\mathrm{m_{SB}} + \mathrm{m}_{BD}}{2} - 1}}{\Gamma(\mathrm{m_{SB}})\Gamma(\mathrm{m}_{BD})(\Omega_{SB}\Omega_{BD})^{\frac{\mathrm{m_{SB}} + \mathrm{m}_{BD}}{2}}} \times K_{\mathrm{m_{SB}} - \mathrm{m}_{BD}}\left(\sqrt{\frac{4v}{\Omega_{SB}\Omega_{BD}}}\right), \tag{6}$$

$$F_{|v|^2}(v) = 1 - \sum_{m=0}^{\mathrm{m_{SB}} - 1} \left(\frac{v}{\Omega_{SB}\Omega_{BD}}\right)^{\frac{\mathrm{m} + \mathrm{m}_{BD}}{2}} \times \frac{2K_{m_{BD} - m}\left(\sqrt{\frac{4v}{\Omega_{SB}\Omega_{BD}}}\right)}{m!\Gamma(\mathrm{m}_{BD})}, \tag{7}$$

respectively, where $K_n(.)$ is the modified Bessel function of the second kind.

III. ERGODIC CAPACITY ANALYSIS

In this section, we derive a closed-form expression for the ergodic capacity (EC) of the proposed NOMA-based symbiotic-radio AmBC system. The instantaneous channel capacities for the three messages, C_{x_l}, are given by [20]

$$C_{x_l} = \log_2(1+\gamma_l), \tag{8}$$

where $l \in \{1,2,3\}$. The EC defined as the expectation of the channel capacity, can be mathematically expressed as [21]

$$EC_{x_l} = \frac{1}{ln2}\int_{\gamma=0}^{\infty} \frac{1}{1+\gamma}\left[1-F_{\gamma_l}(\gamma)\right]d\gamma. \tag{9}$$

The ergodic sum capacity (EC_{sys}) can be expressed as

$$EC_{sys} = EC_{x_1} + EC_{x_2} + EC_{x_3}. \tag{10}$$

In the following subsections, we derive the individual ECs as follows.

A. Ergodic Capacity of x_1

The CDF $F_{\gamma_1}(\gamma)$ can be written as

$$\begin{aligned} F_{\gamma_1}(\gamma) &= 1 - pr(\gamma_1 > \gamma) \\ &= 1 - pr(|h_{SD}|^2 > \frac{\gamma(\beta\rho v+1)}{\rho(a_1-a_2\gamma)}) \\ &= 1 - \underbrace{\Pr(|h_{SD}|^2 > A_1 v + B_1)}_{\phi_1}, \end{aligned} \tag{11}$$

where $A_1 = \frac{\beta\gamma}{(a_1-a_2\gamma)}$ and $B_1 = \frac{\gamma}{\rho(a_1-a_2\gamma)}$. We need to get ϕ_1, which is derived in details in Appendix. By substituting (A.3) and (A.5) into (22) then (9) while taking in our consideration that $0 < \gamma < \frac{a_1}{a_2}$ then we can express EC_{x_1} as in (12) at the top of next page. Using variable transformation of $\tau = \gamma/(a_1 - a_2\gamma)$, EC_{x_1} can be expressed as follows

$$EC_{x_1} = \eta_1 \sum_{m=0}^{m_{SD}-1}\sum_{n=0}^{m}\binom{m}{n}\frac{(\frac{m_{SD}}{\Omega_{SD}})^{m-(n+\frac{\mathrm{m}_{SB}+\mathrm{m}_{BD}}{2})}}{m!(\rho)^{m-n}} J_1, \tag{13}$$

where $\eta_1 = \frac{a_1\beta^{\frac{\mathrm{m}_{SB}+\mathrm{m}_{BD}}{2}}}{ln2\times\Gamma(\mathrm{m}_{SB})\Gamma(\mathrm{m}_{BD})(\Omega_{SB}\Omega_{BD})^{\frac{\mathrm{m}_{SB}+\mathrm{m}_{BD}}{2}}}$, and

$$\begin{aligned} J_1 = &\int_{\tau=0}^{\infty} \frac{(\tau)^{m-(n+\frac{\mathrm{m}_{SB}+\mathrm{m}_{BD}}{2})} e^{\left(\frac{-\tau m_{SD}}{\Omega_{SD}\rho}\right)}}{(1+\tau)(1+a_2\tau)} \\ &\times G_{1,2}^{2,1}\left(\frac{\Omega_{SD}}{\beta\tau m_{SD}\Omega_{SB}\Omega_{BD}}\middle|\begin{matrix}1-(n+\frac{\mathrm{m}_{SB}+\mathrm{m}_{BD}}{2})\\ \frac{\mathrm{m}_{SB}-\mathrm{m}_{BD}}{2},\frac{\mathrm{m}_{BD}-\mathrm{m}_{SB}}{2}\end{matrix}\right)d\tau. \end{aligned} \tag{14}$$

It is noteworthy that to the best of the authors knowledge J_1 does no admit closed-form expression. However, a tight approximation can be found using Gauss Laguerre polynomial [22, Eq. (25.4.45)] by re-defining J_1 as follows

$$J_1 = \int_0^{\infty} e^{-\tau} f(\tau) d\tau, \tag{15}$$

where

$$\begin{aligned} f(\tau) = &e^{\tau}\frac{(\tau)^{m-(n+\frac{\mathrm{m}_{SB}+\mathrm{m}_{BD}}{2})} e^{\left(\frac{-\tau m_{SD}}{\Omega_{SD}\rho}\right)}}{(1+\tau)(1+a_2\tau)} \\ &\times G_{1,2}^{2,1}\left(\frac{\Omega_{SD}}{\beta\tau m_{SD}\Omega_{SB}\Omega_{BD}}\middle|\begin{matrix}1-(n+\frac{\mathrm{m}_{SB}+\mathrm{m}_{BD}}{2})\\ \frac{\mathrm{m}_{SB}-\mathrm{m}_{BD}}{2},\frac{\mathrm{m}_{BD}-\mathrm{m}_{SB}}{2}\end{matrix}\right) \end{aligned} \tag{16}$$

Using [22, Eq. (25.4.45)], we can approximate J_1 as follows

$$J_1 = \sum_{i=1}^{n} w_i f(\tau_i), \tag{17}$$

where τ_i is the i^{th} zero of the Laguerre polynomial, $L_n(x)$, while w_i is the weights that can be calculated as follows:

$$w_i = \frac{(n!)^2 x_i}{(n+1)^2[L_{n+1}(x_i)]^2}. \tag{18}$$

B. Ergodic Capacity of x_2

Similarly, the CDF $F_{\gamma_2}(\gamma)$ can be written as

$$\begin{aligned} F_{\gamma_2}(\gamma) &= 1 - pr(\gamma_2 > \gamma) \\ &= 1 - pr(|h_{SD}|^2 > \frac{\gamma(\beta\rho v+1)}{a_2\rho\gamma}) \\ &= 1 - \underbrace{\Pr(|h_{SD}|^2 > A_2 v + B_2)}_{\phi_2}. \end{aligned} \tag{19}$$

It is noteworthy that ϕ_2 assumes a similar form to ϕ_1, where the same analysis in Appendix can be used. Consequential, EC_{x_2} can be expressed as in (20) at the top of next page. Then using the same variable transformation, we can express it as follows

$$EC_{x_2} = \eta_2 \sum_{m=0}^{m_{SD}-1}\sum_{n=0}^{m}\binom{m}{n}\frac{(\frac{m_{SD}}{\Omega_{SD}a_2})^{m-(n+\frac{\mathrm{m}_{SB}+\mathrm{m}_{BD}}{2})}}{m!(\rho)^{m-n}} J_2, \tag{21}$$

where $\eta_2 = \frac{\beta^{\frac{\mathrm{m}_{SB}+\mathrm{m}_{BD}}{2}}}{ln2\times\Gamma(\mathrm{m}_{SB})\Gamma(\mathrm{m}_{BD})(\Omega_{SB}\Omega_{BD})^{\frac{\mathrm{m}_{SB}+\mathrm{m}_{BD}}{2}}}$, and

$$\begin{aligned} J_2 = &\int_{\gamma=0}^{\infty} \frac{(\gamma)^{m-(n+\frac{\mathrm{m}_{SB}+\mathrm{m}_{BD}}{2})} e^{\left(\frac{-\gamma m_{SD}}{\Omega_{SD}\rho a_2}\right)}}{(1+\gamma)} \\ &\times G_{1,2}^{2,1}\left(\frac{\Omega_{SD}a_2}{\beta\gamma m_{SD}\Omega_{SB}\Omega_{BD}}\middle|\begin{matrix}1-(n+\frac{\mathrm{m}_{SB}+\mathrm{m}_{BD}}{2})\\ \frac{\mathrm{m}_{SB}-\mathrm{m}_{BD}}{2},\frac{\mathrm{m}_{BD}-\mathrm{m}_{SB}}{2}\end{matrix}\right)d\gamma. \end{aligned} \tag{22}$$

Now, we can write

$$J_2 = \int_0^{\infty} e^{-\gamma} f(\gamma) d\gamma, \tag{23}$$

where

$$\begin{aligned} f(\gamma) = &e^{\gamma}\frac{(\gamma)^{m-(n+\frac{\mathrm{m}_{SB}+\mathrm{m}_{BD}}{2})} e^{\left(\frac{-\gamma m_{SD}}{\Omega_{SD}\rho a_2}\right)}}{(1+\gamma)} \\ &\times G_{1,2}^{2,1}\left(\frac{\Omega_{SD}a_2}{\beta\gamma m_{SD}\Omega_{SB}\Omega_{BD}}\middle|\begin{matrix}1-(n+\frac{\mathrm{m}_{SB}+\mathrm{m}_{BD}}{2})\\ \frac{\mathrm{m}_{SB}-\mathrm{m}_{BD}}{2},\frac{\mathrm{m}_{BD}-\mathrm{m}_{SB}}{2}\end{matrix}\right). \end{aligned} \tag{24}$$

$$EC_{x_1} = \frac{1}{ln2}\int_{\gamma=0}^{a_1/a_2} \frac{e^{\left(\frac{-\gamma m_{SD}}{\Omega_{SD}\rho(a_1-a_2\gamma)}\right)} \sum_{m=0}^{m_{SD}-1}\sum_{n=0}^{m}\left(\begin{array}{l}\binom{m}{n}\frac{(\frac{\beta\gamma m_{SD}}{\Omega_{SD}(a_1-a_2\gamma)})^{m-(n+\frac{m_{SB}+m_{BD}}{2})}}{m!}(\frac{1}{\rho\beta})^{m-n} \\ \times G_{1,2}^{2,1}\left(\frac{\Omega_{SD}(a_1-a_2\gamma)}{\beta\gamma m_{SD}\Omega_{SB}\Omega_{BD}}\middle| \begin{array}{c}1-(n+\frac{m_{SB}+m_{BD}}{2}) \\ \frac{m_{SB}-m_{BD}}{2}, \frac{m_{BD}-m_{SB}}{2}\end{array}\right)\end{array}\right)}{(1+\gamma)\Gamma(m_{SB})\Gamma(m_{BD})(\Omega_{SB}\Omega_{BD})^{\frac{m_{SB}+m_{BD}}{2}}} d\gamma. \quad (12)$$

$$EC_{x_2} = \frac{1}{ln2}\int_{\gamma=0}^{\infty} \frac{e^{\left(\frac{-\gamma m_{SD}}{\Omega_{SD}\rho a_2}\right)} \sum_{m=0}^{m_{SD}-1}\sum_{n=0}^{m}\left(\begin{array}{l}\binom{m}{n}\frac{(\frac{\beta\gamma m_{SD}}{\Omega_{SD}a_2})^{m-(n+\frac{m_{SB}+m_{BD}}{2})}}{m!}(\frac{1}{\rho\beta})^{m-n} \\ \times G_{1,2}^{2,1}\left(\frac{\Omega_{SD}a_2}{\beta\gamma m_{SD}\Omega_{SB}\Omega_{BD}}\middle| \begin{array}{c}1-(n+\frac{m_{SB}+m_{BD}}{2}) \\ \frac{m_{SB}-m_{BD}}{2}, \frac{m_{BD}-m_{SB}}{2}\end{array}\right)\end{array}\right)}{(1+\gamma)\Gamma(m_{SB})\Gamma(m_{BD})(\Omega_{SB}\Omega_{BD})^{\frac{m_{SB}+m_{BD}}{2}}} d\gamma. \quad (20)$$

Based on [22, Eq. (25.4.45)], we can write

$$J_2 = \sum_{i=1}^{n} w_i f(\gamma_i), \quad (25)$$

where γ_i is the i^{th} zero of the Laguerre polynomial, $L_n(x)$, while w_i is the weights that can be calculated as in (18).

C. Ergodic Capacity of x_3

The CDF $F_{\gamma_3}(\gamma)$ can be written as

$$\begin{aligned} F_{\gamma_3}(\gamma) &= 1 - pr(\gamma_3 > \gamma) \\ &= 1 - pr(v > \frac{\gamma}{\beta\rho}). \end{aligned} \quad (26)$$

Using (7) and substituting in (9) we can write

$$EC_{x_3} = \frac{1}{ln2}\sum_{m=0}^{m_{SB}-1}\frac{2}{m!\Gamma(m_{BD})}(\frac{1}{\Omega_{SB}\Omega_{BD}\beta\rho})^{\frac{m+m_{BD}}{2}} J_3, \quad (27)$$

where

$$J_3 = \int_{\gamma=0}^{\infty}\frac{(\gamma)^{\frac{m+m_{BD}}{2}}}{1+\gamma}K_{m_{BD}-m}(\sqrt{\frac{4\gamma}{\beta\rho\Omega_{SB}\Omega_{BD}}})d\gamma. \quad (28)$$

Since J_3 can not be solved in terms of elementary functions, we reformulate it using the Meijer's G-functions [23, Eq. (10, 14)], as follows

$$\begin{aligned} J_3 = &\int_{\gamma=0}^{\infty}(\gamma)^{\frac{m+m_{BD}}{2}} G_{1,1}^{1,1}\left(\gamma\middle|\begin{array}{c}0\\0\end{array}\right) \\ &\times G_{0,2}^{2,0}\left(\frac{\gamma}{\beta\rho\Omega_{SB}\Omega_{BD}}\middle|\begin{array}{c}-\\ \frac{m_{BD}-m}{2}, \frac{m-m_{BD}}{2}\end{array}\right) d\gamma. \end{aligned} \quad (29)$$

The integration in (29) can be solved using [23, Eq. (21)], then we can write the closed form of EC_{x_3} as follows

$$\begin{aligned} EC_{x_3} = &\frac{1}{ln2}\sum_{m=0}^{m_{SB}-1}\frac{1}{m!\Gamma(m_{BD})}(\frac{1}{\Omega_{SB}\Omega_{BD}\beta\rho})^{\frac{m+m_{BD}}{2}} \\ &G_{1,3}^{3,1}\left(\frac{1}{\beta\rho\Omega_{SB}\Omega_{BD}}\middle|\begin{array}{c}1-\alpha\\ \frac{m_{BD}-m}{2}, \frac{m-m_{BD}}{2}, 1-\alpha\end{array}\right), \end{aligned} \quad (30)$$

where $\alpha = \frac{m+m_{BD}}{2} + 1$.

IV. RESULTS AND DISCUSSIONS

In this section, we illustrate the derived EC metric, based on which some insights are highlighted. Monte Carlo simulations are generated to corroborate the proposed analysis. Unless mentioned otherwise, the simulation parameters used for generating the plots are given in Table I [16], [24]. To gain more insight into the system performance, we show the relations between EC and other system controlling parameters such as ρ,m_i, a_1, and β. In the following, we denote "Ana" as the exact analytical result, and "Sim" as Monte-Carlo simulation results.

Figure 2 depicted the EC of the three messages and the EC_{sys} versus the SNR where $a_1 = 0.7$, Ω_{SD}=Ω_{SB}=Ω_{BD}=1. We can notice that, both the EC_{x_1} and EC_{x_2} increases slightly in the low-SNR region and remain constants in the high-SNR region due to the saturation of γ_1, γ_2 in (1) and (2). On the other hand, EC_{x_3} continuously increases with the increase in SNR, this result can be deduced by examining (3). Also we can notice that, the performance of EC_{sys} follows the trend of EC_{x_3}. It is noteworthy that both the analytical and the simulation results coincide, which validates our analysis. In the same figure, we investigate the effect of changing the m_i from 1 to 3 on the ECs, it is noteworthy that the EC_{sys} are enhanced when the fading parameters increase.

Figure 3 showed the effect of changing power allocation

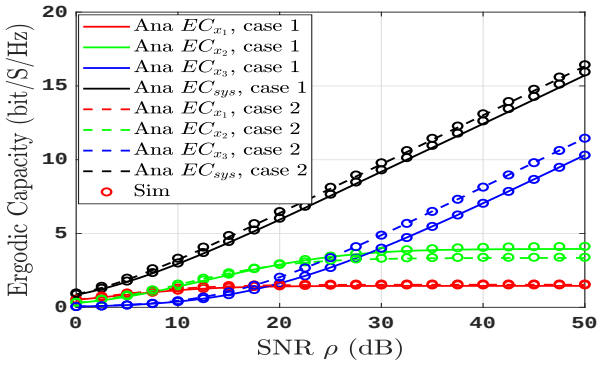

Figure 2. The EC against ρ with $a_1 = 0.7$, Ω_{SD}=Ω_{SB}=Ω_{BD}=1, and $\sqrt{\beta} = 0.2$ while case1 represents ($m_{SD} = m_{SB} = m_{BD} = 1$) and case2 represents ($m_{SD} = m_{SB} = m_{BD} = 3$).

Table I
PARAMETER VALUES USED FOR SIMULATIONS.

Parameter	ρ (dB)	$\sqrt{\beta}$	a_1	Ω_i	γ_{th}	γ_{th2}	m_{SD}	m_{SB}	m_{BD}
value used	0 to 50	0 to 1	0.5 to 0.99	0.75 to 3	1	0.1	4	1	1

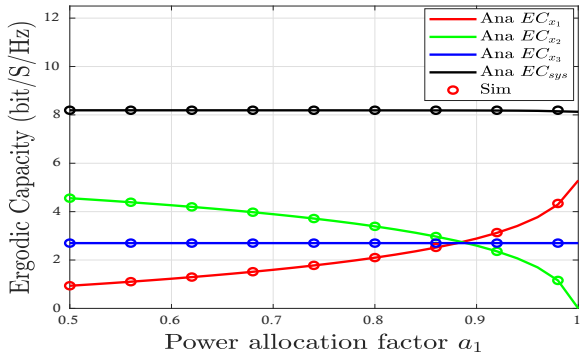

Figure 3. The EC against power allocation coeff. a_1 with $\sqrt{\beta} = 0.2$ and $\rho = 25$ dB.

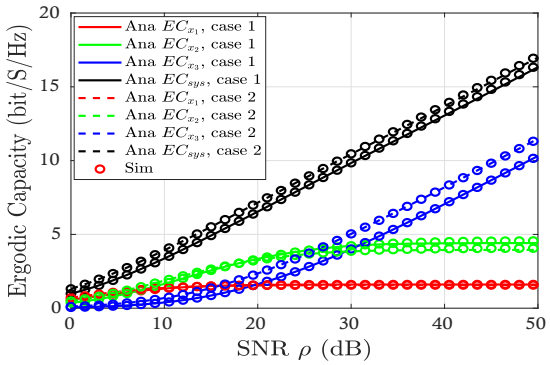

Figure 5. The EC against ρ with $a_1 = 0.7$, $\sqrt{\beta} = 0.2$. Case1 (Ω_{SD}=Ω_{SB}=Ω_{BD}=1), case2 (Ω_{SD}=Ω_{SB}=Ω_{BD}=1.5.)

factor a_1 on the EC with $\rho = 25$ dB and $\sqrt{\beta} = 0.2$. Specifically, we provide the curves of the EC_{x_i} and EC_{sys} versus a_1 to get insights about the effectiveness and the fairness. From the figure, we notice that EC_{x_1} increases with the increase in a_1 since the large a_1 means the high SINR according to (1), while EC_{x_2} decreases with the increase in a_1 since the SINR decreases based on (2). On the other hand EC_{x_3} remains constant because the BD reflects all transmit power from the BS, and independent of a_1. Finally, we can notice that EC_{sys} is fixed over all values of a_1, this is due to that the rate of the increase in EC_{x_1} is the same as the rate of the decrease in EC_{x_2}.

Figure 4 demonstrated the effect of the reflection coefficient $\sqrt{\beta}$ on the EC_{x_i} and EC_{sys} assuming $a_1 = 0.7$ and Ω_{SD}= Ω_{SB}=Ω_{BD}=1. The results indicates an improvement in the EC of backscatter message EC_{x_3} with higher β and this trend is due to the enhancement of γ_3 in (3), while the situation is different for EC of both source messages EC_{x_1} and EC_{x_2}, as γ_1 and γ_2 degrade with higher value of β as it is clear from (1) and (2).

In Fig. 5 we illustrated the effect of changing the expectations of the channels gains Ω_i on the EC_{x_i} and EC_{sys} assuming $a_1 = 0.7$ and $\Omega_{SD} = \Omega_{SB} = \Omega_{BD} = 1$ in case1 while in case2 Ω_{SD}=Ω_{SB}=Ω_{BD}=1.5. It is noteworthy that with the increase of the expectations, the interference terms in both γ_1 and γ_2 increase, which leads to the deterioration of there ergodic capacities. On the other hand, due to the SIC, γ_3 is enhanced as well as its EC.

To evaluate the performance of the proposed system in this work, we compared its performance with a benchmark scheme; the OMA-based SR-AmBC system; in terms of ergodic capacity. Figure 6 compares the performance of EC_{x_i} and EC_{sys} for both systems under the same values of system parameters. The figure illustrates that the proposed system based on NOMA outperformed its counterpart based on OMA for the EC_{x_i} of each individual messages and EC_{sys} as well.

V. CONCLUSIONS

In this paper, we introduced a downlink NOMA-based SR-AmBC system under Nakagami-m fading channels. We derived new analytical closed-form expressions for the ECs. The validity of the derived analytical expressions are confirmed

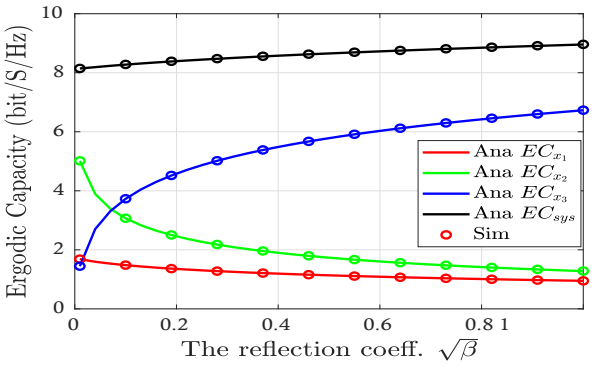

Figure 4. The EC against $\sqrt{\beta}$ at $\rho = 25$ dB and $a_1 = 0.7$.

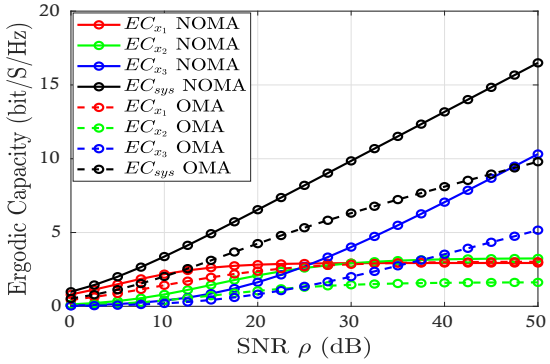

Figure 6. The EC of proposed system under different schemes NOMA and OMA for $\sqrt{\beta} = 0.04$ and $a_1 = 0.7$.

through Monte-Carlo simulations. Besides, we discussed the influence of different parameters on the the ECs. At the end of our results, we held a comparison with a benchmark system, from which we concluded that the NOMA-based SR-AmBC system outperformed the OMA-based benchmark system.

REFERENCES

[1] Z. Wei, L. Yang, D. W. K. Ng, J. Yuan, and L. Hanzo, "On the performance gain of NOMA over OMA in uplink communication systems," *IEEE Trans. Commun.*, vol. 68, no. 1, pp. 536–568, 2020.

[2] B. M. ElHalawany, F. Jameel, D. B. da Costa, U. S. Dias, and K. Wu, "Performance analysis of downlink NOMA systems over κ-μ shadowed fading channels," *IEEE Trans. Veh. Technol.*, vol. 69, no. 1, pp. 1046–1050, 2020.

[3] N. Van Huynh, D. T. Hoang, X. Lu, D. Niyato, P. Wang, and D. I. Kim, "Ambient backscatter communications: A contemporary survey," *IEEE Commun. Surveys Tuts.*, vol. 20, no. 4, pp. 2889–2922, 2018.

[4] B. Liu, S. Han, H. Peng, Z. Xiang, G. Sun, and Y.-C. Liang, "A cross-layer analysis for full-duplex ambient backscatter communication system," *IEEE Wireless Commun. Lett.*, vol. 9, no. 8, pp. 1263–1267, 2020.

[5] U. S. Toro, B. M. ElHalawany, L. WANG, and K. Wu, "Machine learning assisted signal detection in ambient backscatter communication networks," *IEEE Netw.*, vol. 68, no. 1, pp. 536–568, 2021.

[6] W. U. Khan, M. A. Javed, T. N. Nguyen, S. Khan, and B. M. Elhalawany, "Energy-efficient resource allocation for 6G backscatter-enabled NOMA iov networks," *IEEE Trans. Intell. Transp. Syst.*, pp. 1–11, 2021.

[7] R. Long, Y.-C. Liang, H. Guo, G. Yang, and R. Zhang, "Symbiotic radio: A new communication paradigm for passive internet of things," *IEEE Internet Things J.*, vol. 7, no. 2, pp. 1350–1363, 2020.

[8] F. Jameel, S. Zeb, W. U. Khan, S. A. Hassan, Z. Chang, and J. Liu, "NOMA-enabled backscatter communications: Toward battery-free IoT networks," *IEEE Internet of Things Mag.*, vol. 3, no. 4, pp. 95–101, 2020.

[9] W. Chen, H. Ding, S. Wang, D. B. da Costa, F. Gong, and P. H. J. Nardelli, "Ambient backscatter communications over NOMA downlink channels," *China Commun.*, vol. 17, no. 6, pp. 80–100, 2020.

[10] Q. Zhang, L. Zhang, Y.-C. Liang, and P.-Y. Kam, "Backscatter-NOMA: A symbiotic system of cellular and internet-of-things networks," *IEEE Access*, vol. 7, pp. 20 000–20 013, 2019.

[11] X. Li, M. Zhao, M. Zeng, S. Mumtaz, V. G. Menon, Z. Ding, and O. A. Dobre, "Hardware impaired ambient backscatter NOMA systems: Reliability and security," *IEEE Trans. Commun.*, vol. 69, no. 4, pp. 2723–2736, 2021.

[12] X. Li, M. Zhao, Y. Liu, L. Li, Z. Ding, and A. Nallanathan, "Secrecy analysis of ambient backscatter NOMA systems under I/Q imbalance," *IEEE Trans. Veh. Technol.*, vol. 69, no. 10, pp. 12 286–12 290, 2020.

[13] X. Li, Y. Zheng, W. U. Khan, M. Zeng, D. Li, G. K. Ragesh, and L. Li, "Physical layer security of cognitive ambient backscatter communications for green internet-of-things," *IEEE Trans. Green Commun. Netw.*, vol. 5, no. 3, pp. 1066–1076, 2021.

[14] M. Elsayed, A. Samir, A. A. A. El-Banna, X. Li, and B. M. ElHalawany, "When NOMA multiplexing meets symbiotic ambient backscatter communication: Outage analysis," *IEEE Transactions on Vehicular Technology*, vol. 71, no. 1, pp. 1026–1031, 2022.

[15] R. Ramesh, S. Gurugopinath, and S. Muhaidat, "Outage performance of relay-assisted single- and dual-stage NOMA over power line communications," *IEEE Access*, vol. 9, pp. 86 358–86 368, 2021.

[16] Y. Ni, Y. Liu, Q. Wang, Y. Wang, H. Zhao, and H. Zhu, "Vehicular networks under Nakagami-m fading channels: Outage probability and ergodic achievable rate," *IEEE Access*, vol. 8, pp. 121 501–121 512, 2020.

[17] X. Gong, X. Yue, and F. Liu, "Performance analysis of cooperative NOMA networks with imperfect CSI over Nakagami-m fading channels," *Sens.*, vol. 20, no. 2, 2020. [Online]. Available: https://www.mdpi.com/1424-8220/20/2/424

[18] U. Fernandez-Plazaola, L. Moreno-Pozas, F. J. Lopez-Martinez, J. F. Paris, E. Martos-Naya, and J. M. Romero-Jerez, "A tractable product channel model for line-of-sight scenarios," *IEEE Trans. on Wireless Commun.*, vol. 19, no. 3, pp. 2107–2121, 2020.

[19] R. E. Gaunt, "Products of normal, beta and gamma random variables: Stein operators and distributional theory," 2016.

[20] A. Rauniyar, P. Engelstad, and O. N. Østerbø, "Ergodic capacity performance of NOMA-SWIPT aided iot relay systems with direct link," in *2020 18th International Symposium on Modeling and Optimization in Mobile, Ad Hoc, and Wireless Networks (WiOPT)*, 2020, pp. 1–8.

[21] B. M. ElHalawany, A. A. Aziz El-Banna, and K. Wu, *Physical-Layer Security for Ambient Backscattering Internet-of-Things*. Cham: Springer International Publishing, 2021, pp. 25–37.

[22] M. Abramowitz and I. A. Stegun, Eds., *Handbook of Mathematical Functions with Formulas, Graphs and Mathematical Tables*. New York: Dover Publications, Inc., 1965.

[23] V. S. Adamchik and O. I. Marichev, "The algorithm for calculating integrals of hypergeometric type functions and its realization in reduce system," in *Proceedings of the International Symposium on Symbolic and Algebraic Computation*, ser. ISSAC '90. New York, NY, USA: Association for Computing Machinery, 1990, p. 212–224. [Online]. Available: https://doi.org/10.1145/96877.96930

[24] B. Tahir, S. Schwarz, and M. Rupp, "Analysis of uplink IRS-assisted NOMA under Nakagami-m fading via moments matching," *IEEE Wireless Commun. Lett.*, vol. 10, no. 3, pp. 624–628, 2021.

APPENDIX

$$\phi = \int_0^\infty \int_{Av+B}^\infty f_{|h_{SD}|^2}(x) f_v(v) dx dv. \tag{A.1}$$

By substituting (5), (6) into (A.1), ϕ is expressed as

$$\phi = \int_0^\infty (e^{\left(\frac{-m_{SD}}{\Omega_{SD}}(Av+B)\right)} \sum_{m=0}^{m_{SD}-1} \frac{((m_{SD}/\Omega_{SD})(Av+B))^m}{m!} \times \frac{2v^{\frac{\mathrm{m_{SB}}+\mathrm{m}_{BD}}{2}-1} K_{\mathrm{m_{SB}}-\mathrm{m}_{BD}}(\sqrt{\frac{4v}{\Omega_{SB}\Omega_{BD}}})}{\Gamma(\mathrm{m_{SB}})\Gamma(\mathrm{m}_{BD})(\Omega_{SB}\Omega_{BD})^{\frac{\mathrm{m_{SB}}+\mathrm{m}_{BD}}{2}}} dv. \tag{A.2}$$

Using binomial expansion we can get,

$$\phi = \theta \sum_{m=0}^{m_{SD}-1} \frac{(m_{SD}A/\Omega_{SD})^m}{m!} \sum_{n=0}^{m} \binom{m}{n} (\frac{B}{A})^{m-n} \times \underbrace{\int_0^\infty e^{\frac{-m_{SD}Av}{\Omega_{SD}}} v^{n+\frac{m_{SB}+m_{BD}}{2}-1} K_{m_{SB}-m_{BD}}(\sqrt{\frac{4v}{\Omega_{SB}\Omega_{BD}}}) dv}_{I_1}, \tag{A.3}$$

where $\theta = \frac{2e^{\left(\frac{-Bm_{SD}}{\Omega_{SD}}\right)}}{\Gamma(\mathrm{m_{SB}})\Gamma(\mathrm{m}_{BD})(\Omega_{SB}\Omega_{BD})^{\frac{\mathrm{m_{SB}}+\mathrm{m}_{BD}}{2}}}$. Since I_1 in (A.3) can not be solved in terms of elementary functions, we reformulate it based on Meijer's G-functions [23, Eq. (11, 14)], as follows,

$$I_1 = 0.5 \int_0^\infty v^{n+\frac{m_{SB}+m_{BD}}{2}-1} G_{0,1}^{1,0}\left(\frac{-m_{SD}Av}{\Omega_{SD}} \middle| \begin{matrix} - \\ 0 \end{matrix}\right) \times G_{0,2}^{2,0}\left(\frac{v}{\Omega_{SB}\Omega_{BD}} \middle| \begin{matrix} - \\ \frac{m_{SB}-m_{BD}}{2}, \frac{m_{BD}-m_{SB}}{2} \end{matrix}\right) dv, \tag{A.4}$$

which can be solved using [23, Eq. (21)] as follows

$$I_1 = 0.5(\frac{m_{SD}A}{\Omega_{SD}})^{-(n+\frac{m_{SB}+m_{BD}}{2})} \times G_{1,2}^{2,1}\left(\frac{\Omega_{SD}}{m_{SD}A\Omega_{SB}\Omega_{BD}} \middle| \begin{matrix} 1-(n+\frac{m_{SB}+m_{BD}}{2}) \\ \frac{m_{SB}-m_{BD}}{2}, \frac{m_{BD}-m_{SB}}{2} \end{matrix}\right). \tag{A.5}$$